ALMA MATER STUDIORUM-UNIVERSITÁ DI BOLOGNA

FACOLTÀ DI INGEGNERIA E ARCHITETTURA - CAMPUS DI CESENA
Corso di Laurea Magistrale in Ingegneria Biomedica

Descrizione e analisi quantitativa dei meccanismi di gestione del calcio intracellulare nei cardiomiociti derivati da staminali pluripotenti indotte

Tesi in:
Bioingegneria Molecolare e Cellulare

Relatore:
Stefano Severi

Candidato:
Dario Cori

Correlatore:
Michelangelo Paci

Anno Accademico 2016/2017 - II Sessione

Sommario

L'obiettivo di questa tesi è quello di migliorare l'attuale formulazione del primo modello finora sviluppato di cardiomiociti derivati da hiPSC, il Paci2013, attraverso l'utilizzo: i) di un set di dati sperimentali di transienti di Ca^{2+} e ii) di una procedura automatica per l'ottimizzazione dei parametri del modello.

Il lavoro svolto per questa tesi si articola in diverse fasi. Dapprima è stata introdotta nel modello una nuova formulazione del rilascio di Ca^{2+} dal reticolo sarcoplasmatico che riproduce in maniera più realistica un importante fenomeno alla base della contrazione muscolare cardiaca. Successivamente è stata effettuata una discriminazione dei dati sperimentali dei transienti di Ca^{2+} tramite una procedura di classificazione non supervisionata al fine di rendere il set di misure sperimentali più consitente con il modello in esame. In seguito è stato implementato un framework di ottimizzazione parametrica che, tramite la minimizzazione di una funzione costo, ha consentito di calibrare il modello sulla base dei dati sperimentali. Infine, in fase di validazione del modello, sono state effettuate delle simulazioni di bloccanti di corrente per valutare che gli effetti di tali bloccanti sul potenziale d'azione fossero consistenti con dati sperimentali da letteratura .

In conlusione, questo lavoro di tesi tesi ha fornito *in primis* una nuova versione del modello Paci2013 calibrata su dati sperimentali di transienti di Ca^{2+} ed inoltre il framework di ottimizzazione parametrica, che rappresenta uno strumento utile per lo sviluppo di modelli computazionali.

Keywords

Human Induced Pluripotent Stem Cell

Computational Modelling

Action Potential

Calcium Transient

Parameter Tuning

Acronyms

AP	Action Potential
APA	Action potential amplitude
APD	Action potential duration
APD_{xx}	Action potential duration at xx% of repolarization
MDP	Maximum diastolic potential
TP	Time to peak
RT1090	rise time that occurs to rise from the 10% to the 90% of Ca^{2+} transient amplitude
DT9010	decay time that occurs to decay from the 90% to the 10% of Ca^{2+} transient amplitude;
RS1090	average rise slope from 10% to the 90% of Ca^{2+} transient amplitude
DS9010	average decay slope from 90% to the 10% of transient amplitude
CM	Cardiomyocite
EC	Excitation/contraction
hESC	Human embryonic stem cell
hESC-CM	human embryonic stem cell-derived Cardiomyocyte

hiPSC	Human induced pluripotent stem cell
hiPSC-CM	human induced Pluripotent stem cell-derived Cardiomyocyte
TTX	Tetrodotoxine
Nifed	Nifedipine
SR	Sarcoplasmic reticulum
LQTS	Long QT syndrome
$\mathbf{I_{K1}}$	inward rectifier K^+ current
$\mathbf{I_{Na}}$	Na^+ current
$\mathbf{I_{NaL}}$	L-type Na^+ current
$\mathbf{I_{Kr}}$	rapid delayed rectifier K^+ current
$\mathbf{I_{Ks}}$	slow delayed rectifier K^+ current
$\mathbf{I_{CaL}}$	L-type Ca^{2+} current
$\mathbf{I_{CaT}}$	T-type Ca^{2+} current
$\mathbf{I_{to}}$	transient outward K^+ current
$\mathbf{I_f}$	funny current
$\mathbf{I_{NaK}}$	Na^+ /K^+ pump
$\mathbf{I_{NaCa}}$	Na^+ /Ca^{2+}
$\mathbf{I_{pCa}}$	sarcolemmal Ca^{2+} -ATPase current
$\mathbf{I_{bCa}}$	background Ca^{2+} current
$\mathbf{I_{up}}$	sarcoplasimc reticulum uptake current
$\mathbf{I_{rel}}$	sarcoplasmic reticulum release current
$\mathbf{I_{leak}}$	sarcoplasmic reticulum leakage current

$\mathbf{I_{stim}}$	stimulus current

Contents

CHAPTER I

Introduction: general overview about stem cell technology and the cardiac modelling

In this chapter, an introduction about the stem cell is presented in order to give the basic information about the wide world of the stem cell technology. Later on, another introduction about the cardiac modelling is exposed, in particular the Hodgkin-Huxley modelling paradigm. The aim is to provide the essential information to understand the work presented in the next chapters

I.1 The stem cells

Stem cells are non-specialized cells, present in all the pluricellular organism and capable to transform into other different specialized cells though a biological process called cellular differentiation.

We can give this formal definition: “a stem cell is a cell that can continuously produce unaltered daughters and has the ability to produce daughter cells that have different, more restricted properties"[1]. Thus, two fundamental properties can be defined:

- *self-renewal:* the ability to generate, through several division cycles, at least one daughter equivalent to the mother cell with latent capacity of

differentiation[1].

- *potency:* the capacity to become, under some physiologic or experimental conditions, tissue or organ specific cell with certain properties[1].

So, different levels of stem cell potency, can be defined[2]:

- Totipotent: derive from the fusion of an egg cell and a sperm cell. They are able to form the entire organism since they can differentiate into embryonic and extra-embryonic cell type, i. e. all the lineages needed to build the whole organism;
- Pluripotent: they are able to differentiate only into the embryonic cell types, so they can form all the body cell lineage;
- Multipotent: can differentiate into the cell types of a organic tissue;
- Oligopotent: able to differentiate into two or more lineages within a tissue;
- Unipotent: can develop into only a single cell lineage;

Stem cells can be distinguished in *adult* and *embryonic*. Adult stem cells are present in some of our organs and tissues, such as spinal cord, and their task is to regenerate the tissue or organ itself; they can be *pluri*, *multi* or *unipotent*. Embryonic stem cells are derived from an embyro that develops after an *in-vitro* fertilization of an egg cell (FigureI.1). In 1998 *Thomson et al.* [3] were the first ones to succeed in this procedure. After the fertilization of the human oocyte and through a process called *cleveage*, a rapid division of the zygote, a cluster of totipotent cells is produced. Then, passing through the *morula* state, it reaches the *blastocyst* stage, in which two primary elements are present:

- *Trophloblast;*
- *Inner-cell mass;*

Then, slightly more than 2 weeks after the fertilization, a process called *gastrulation* occurs on the inner cell mass. Through this process the 3 germ layers are generated, each of them capable to differentiate into a limited number of phenotypes:

- *Endoderm*, the internal layer, that differentiates into tissues such as hepatic, pulmonary, vesical *etc*;
- *Mesoderm*,the intermediate layer, that differentiates into bone, muscular, cardiac tissues, *etc*;
- *Endoderm*,the external layer, that differentiates into dermal, nervous tissues, *etc*;

The human embryonic stem cells (hESCs) are obtained by isolating the cells from the inner cell mass of blastocyst and they can differentiate into the tissues produced by the three germ layers (FigureI.1). Thanks to their pluripotency, hESCs could be the starting point to develop a novel therapeutic approach for many diseases, such as cancer, but, on the other hand, they could also raise some controversy concerning their proper ethical use.

I.2 Human induced pluripotent stem cell

Human induced pluripotent stem cells (hiPSCs) are pluripotent cells obtained by reprogramming the DNA of human somatic cells. They have the same properties of hESCs, such as self-renewal and potency, but they bring some new advantages:

- There are no ethical issues, since no human embryos are used;
- It is possible to create a stem cell culture for a specific patient because hiPSCs are obtained safely from a patient (for example from a skin biopsy). This reduces the risk of rejection in case of transplant;

The first experimental trials to produce hiPSCs were performed [4][5] introducing in the human adult dermal fibroblast 4 different reprogramming genes through lentiviral vectors. These are: Oct-3/4, Sox2, Klf4, c-Myc.

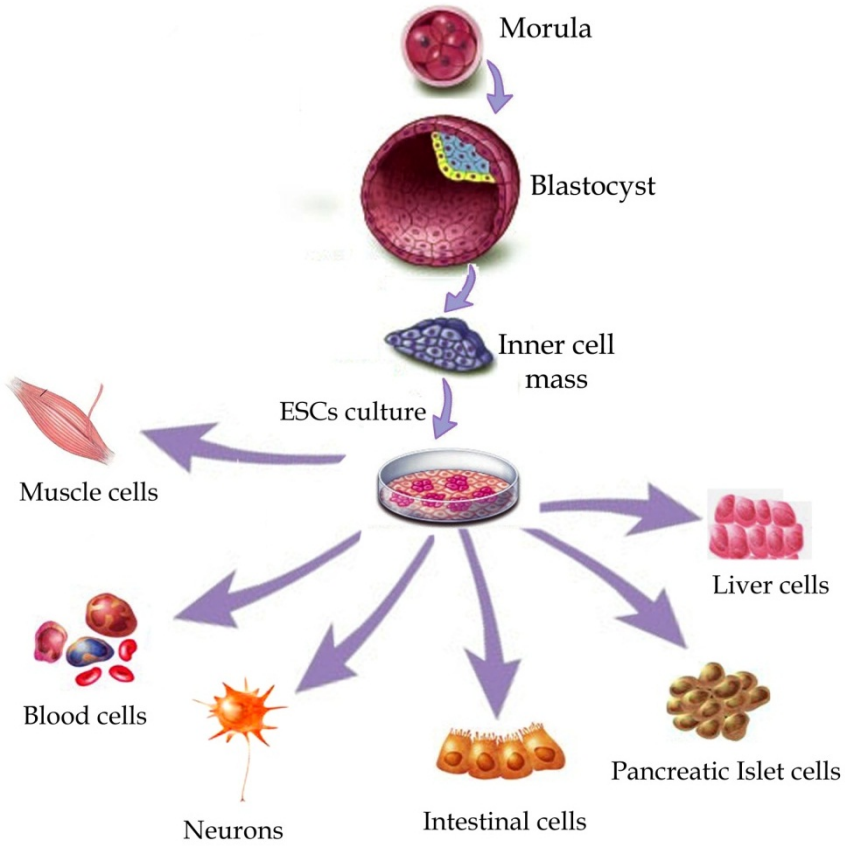

Figure I.1: Differentiation process of stem cells; image adapted from [6]

After 2- 3 week in culture it occurs the loss of their tissue-specific properties until they return to be pluripotent in a state that is like hESC. Then they can be differentiated into several phenotypes. This approach opens a wide range of promising new medical therapies (FigureI.2)

- Regenerative medicine;
- Creation of pathology-specific cell models that can be used for research and development of new drugs;
- Production of patient-specific healthy somatic cells;

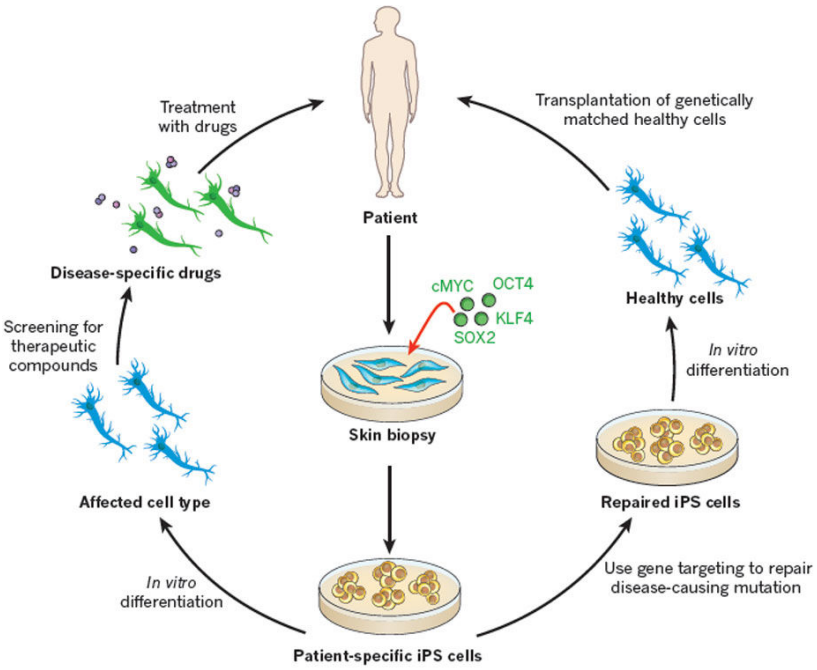

Figure I.2: Application of hiPSC; image adapted from [7]

I.3 Stem cell differentiation into cardiomyocytes

There are several methods that can differentiate human pluripotent stem cell into cardiomyocytes [8]. One of them, called hanging drop method, consist in inducing hESCs and hiPSCs to the spontaneous differentiation into CMs through the formation of a particular 3 dimensional aggregates of pluripotent cells, called Embryoid Bodies. These are obtained by dissociating pluripotent stem cells into small clusters and then removing them from the environment supporting their undifferentiated state. After few days from the formation of EBs, they are plated on cultured plates. Then, in about one day, spontaneous beating areas on the culture can be observed, establishing the differentiation into the cardiomyocytes.

Another method consists in adding to the stem cell culturing mouse endodermal-like cells. These one will secrete a differentiation inducing factor which is still under studies because it is not fully understood yet. One more method is based on using grow factors which induce the differentiation into

mesodermal-like and endodermal-like cells, since the first is the responsible of the formation of cardiac tissue and the latter is responsible of the signal generating tissue[10].

Unfortunately, all these methods have a very low efficiency: cultures with mouse endodermal-like cells have an efficiency between 2.9%-9.4% and cultures with EBs methods have efficiency between 1.6%-12.5%. So, better differentiation methods should be found to let the hESCs and hiPSCs be usable tools for future cell therapies and pharmacological studies.

Furthermore, as stated before, with hiPSCs it is possible to replicate not only cells from healthy donors, but also from subjects carrying particular genetic mutations, giving the opportunity to make accurate and patient-specific in vitro studies of that specific pathology. Currently, many studies are focused on the Long QT syndrome(LQTS). As the name suggests, subjects affected by this pathology are characterized by a long QT interval on the ECG due to an abnormal prolongation of the ventricular repolarization. This disease leads to an abnormal heartbeat and may cause syncope, faintness and ventricular fibrillation[11]. Different gene mutations cause LQTS and some of them are under investigation by using hiPSCs culture from LQTS positive patients:

- LQT1, affecting the KCNQ1 gene that encode for the repolarizing slow delayed rectifier current (I_{Ks}) channel, causing its loss-of-function;
- LQT2, mutating the KNCH2 gene that encode for the fast-delayed rectifier current (I_{Kr}) channel, causing its loss-of-function;
- LQT3, which mutates the SCN5A gene which encodes for the depolarizing sodium current (I_{Na}), causing its gain-of-function, and, in particular, an inward Na^+ leakage during the repolarization of the membrane potential;
- LQT8 (Timothy syndrome) in which CACNA1C gene encoding the L-type Ca^{2+} current (I_{CaL}) channel mutates, causing a delay in the closure of the I_{CaL} channels;

I.4 The cardiac action potential

An ction potential(AP) consists in the rapid membrane potential depolarization-repolarization sequence as a consequence of an external stimulus or spontaneously triggered.

The cardiac muscle is a highly organized structure and his functional unit, responsible of the contraction, is the cardiomyocyte (CM). There is also a little part of them, called peacemakers cells, able to the spontaneously generate an AP, thus giving the heart a self-contracting property.

As shown in[12], the excitation-contraction (EC) coupling in the myocardial tissue is started by the AP generated from the peacemaker cells. When the AP reaches a contractile cell causing its membrane depolarization, due to the ion current transfer, the Ca^{2+} intracellular concentration increases. This Ca^{2+} increase starts, with the activation of the myofilaments, the cross-bridge mechanism resulting in the cell shortening. All the CMs should be very coordinated during the heart beating in order to have an efficient pumping action and a proper body perfusion. The heart electric activity can be recorder through ECG. The ECG track represent the sum of the whole APs generated by the CMs, since the AP assumes different waveform according to the location in the heart where it is recorded (FigureI.3).

The most representative shape is the ventricular one and this will be used to explain the mechanism behind the cardiac AP. The AP waveform can be divided in 5 phases (FigureI.4) corresponding to different activation and inactivation of ionic currents and pumps:

- *phase 4:* the membrane potential is kept stable at about -90 mV by different mechanism:
  - The inward rectifier K^+ current I_{K1} that causes a flux of K^+ ions, whose equilibrium potential primary defines the CM membrane potential;
  - The ATP-based Na^+/K^+ pump (I_{NaK}) which transports 3 Na^+ ions toward the extracellular space and brings 2 K^+ ions into the intracellular compartment, thus generating a outward current;

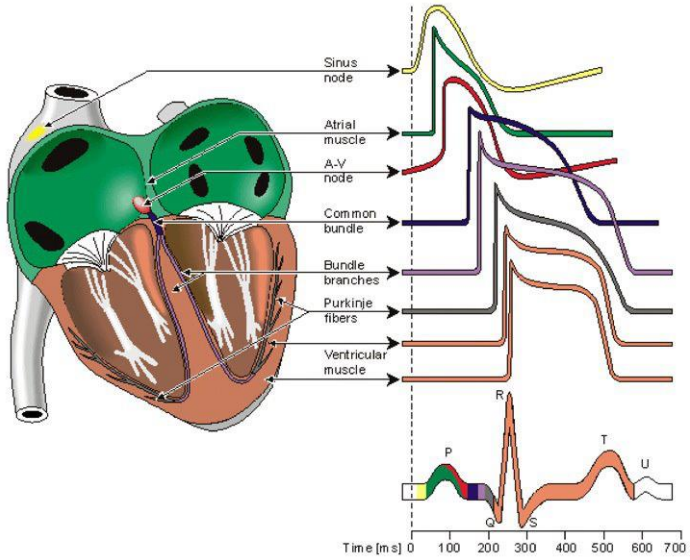

Figure I.3: AP genesis from different cardiac regions.; image adapted from [13]

  - The bidirectional Na^+/Ca^{2+} exchanger (I_{NaCa}) which allows the exchange of 1 Ca^{2+} ion for 3 Na^+ ions dependently to the concentration gradient; together with the Ca^{2+} ATP-ase (I_{pCa}) it balance the intracellular Ca^{2+} concentration and consequently keeps the resting potential;

- *Phase 0*: when the CM membrane potential reaches a voltage threshold at about -60 mV it increases shortly to 40-50 mV resulting in an upstroke. This potential steep slope is due to Na+ current (I_{Na}), a fast Na^+ influx following the electrochemical Na^+ gradient along the membrane;

- *Phase 1*: I_{Na} rapidly inactivate while a transitory outward K^+ current (Ito) activates that causes a transient K^+ efflux along the electrochemical gradient; in the ventricular cells Ito induces the typically spike-and-dome shape;

- *Phase 2:* the I_{CaL} reaches its peak and sustains the AP plateau. This current activates previously during the upstroke but reaches its maxi-

mum during the plateau since it has a slower dynamic than I_{Na};

- *Phase 3:* represents the repolarization of the membrane potential and it is induced by the rapid delayed rectifier K^+ current (I_{Kr}) and the slow delayed rectifier K^+ current (I_{Ks});

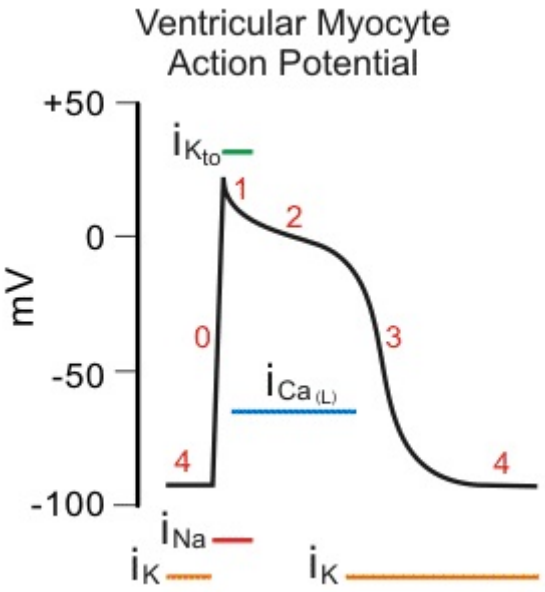

Figure I.4: Ventricular AP phases; image adapted from [13]

Since this thesis deals with the calcium handling during the AP It is worth to spend more words about Ca^{2+} physiological role during the contraction mechanism and how can an AP trigger the CM contraction. There are some elements involved in this phenomenon: The L-type Ca^{2+} channels, the T-tubules, the sarcoplasmic reticulum (SR) and the sarcomeres. SR represents a structure inside the cytosol where the Ca^{2+} is stored at high concentration and it has two main channels to communicate with the cytosol: Serca-2 pump (Ca^{2+} intake) and the Ca^{2+} ryanodine-sensitive release channels. Its role it to regulate the cytosolic Ca^{2+} concentration. T-Tubules are specialized structure which let the L-type Ca^{2+} channels and the SR Ca^{2+} discharge system to be close to each other. The sarcomere represents the cell contractile unit, composed by actin and myosin filaments, which will shorten in presence of Ca^{2+} (cross-bridge mechanism).

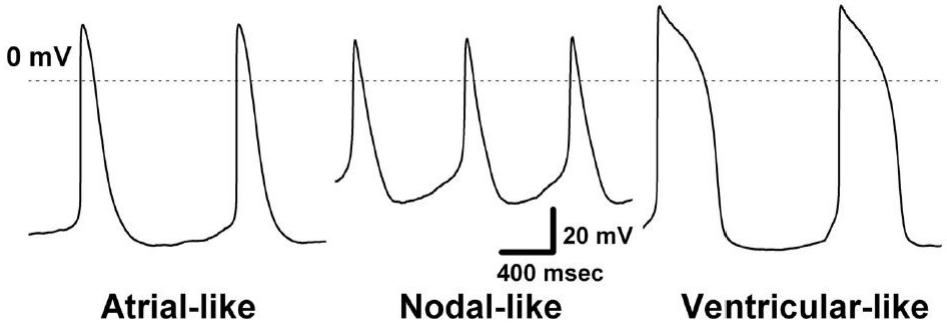

Figure I.5: hiPSC-CM spontaneous APs from different cell classes.; image adapted from [16]

I_{CaL} channels open when the AP fires, but the small amount of Ca^{2+} isn't enough to trigger the crossbridge mechanism. But this small amount of Ca^{2+} is sufficient to trigger Ca^{2+} release from SR, in a positive feedback process called Calcium Induced Calcium Released (CICR), which increases the intracellular Ca2+ concentration by about 100-fold, allowing the cellular contraction [14]

In order to keep the intracellular Ca2+ concentration at adequate levels, ATP-dependent SERCA pump moves Ca^{2+} from cytosol back to the SR and I_{NaCa}, together with I_{pCa}, extrudes Ca^{2+} towards the extracellular space. Cardiomyocytes derived from hESCs (hESC-CMs) or hiPSCs (hiPSC-CMs) behave like not fully mature cardiomyocytes, thus showing partly different AP shapes compared to adult myocytes. The main differences concern the spontaneous APs, a feature present in hESC-CMs and hiPSC-CMs but only in adult nodal cells, and some morphological features such as the more positive Maximum Diastolic Potential(MDP), that is the most negative transmembrane potential, or the smaller Maximum Upstroke Velocity ($\frac{dV}{dtmax}$,that is the maximum value of the slope during the upstroke[15][16]. Another aspect regards the more heterogeneous AP shapes shown by hESC-CMs and hiPSC-CMs: they can still be classified among ventricular-atrial and nodal-like according to their similarity to the respective adult phenotype, but they show higher variability of their electrophysiological properties (FigureI.5).

I.5 Action Potential modelling: the Hodgkin-Huxley paradigm

Since during this thesis work the Hodgkin-Huxley (HH) modelling paradigm was mainly used, a short summary of its fundamental equations is here provided. The HH model is mathematical model describing the generation and propagation of the neuronal AP and it is one of the most successful mathematical models of a complex biological process that has ever been formulated [18][17]. Despite the original HH model was formulated for one specific cellular species, the HH modelling paradigm is used also to describe adequately a generic AP and, in our case, the cardiac AP.

The fundamental equation used to obtain the AP expression as a function of time, i.e. the evolution in time of the transmembrane potential $V_m(t)$, is:

$$\frac{dV_m}{dt} = \frac{I_{ion}}{C_m} \tag{I.1}$$

where I_{ion} is the sum of all the ionic currents and C_m is the membrane capacitance.

The mathematical equation used to describe the generic ionic current flowing through the membrane is:

$$I = x^a * y^b * G_{max} * (V_m - E_r) \tag{I.2}$$

where $G_{max}$is the maximum channel conductance, E_r is the resting potential for a specific ionic species and is computed as Nerst potential as follows:

$$E_r = \frac{RT}{zF} * \ln \frac{[ion]_o}{[ion]_i} \tag{I.3}$$

$x(V_m,t)$ and $y(V_m, t)$ are the gating variables, respectively the activation and inactivation gating variable. The meaning of these can be explained considering that the ionic current amplitude is proportional to the open gates in that specific channel. A generic gating variable describe the fraction of the open (and the closed) gates, so it will be always inside the range [0, 1]. The

transition from open to closed and vice versa is described by this formulation:

$$\frac{dx}{dt} = \alpha_x * (1 - x) - \beta_x * x \tag{I.4}$$

If the values of α_{x} and β_{x} depend on $\mathrm{V_m}$, then the state of the gating variable is voltage dependent. This means that activation gates will have a value proportionally dependent to the membrane depolarization while the inactivation gates will have a value inversely proportional to the membrane depolarization.

Imposing:

$$\alpha_x = \frac{x_{\mathrm{inf}}}{\tau_x} \tag{I.5}$$

and

$$\beta_x = \frac{(1 - x_{\mathrm{inf}})}{\tau_x} \tag{I.6}$$

Equation I.4 can be reformuled as:

$$\frac{dx}{dt} = \frac{x_{\mathrm{inf}} - x}{\tau_x} \tag{I.7}$$

where the stady state

$$x_{\mathrm{inf}} = \frac{\alpha_x}{\alpha_x \pm \beta_x} \tag{I.8}$$

represents the value at which x tends at certain membrane voltage and it is experimentally obtained by fitting data using the following sigmoid function:

$$x_{\mathrm{inf}} = \frac{1}{1 + \exp^{\frac{V_m - V_h}{K}}} \tag{I.9}$$

In this new representation of x_{inf}, $\mathrm{V_h}$ is the voltage of half activation and K is the gradient of activation. The time constant:

$$\tau_x = \frac{1}{\alpha_x + \beta_x} \tag{I.10}$$

measures the velocity of the gating variable x to reach its steady state.

CHAPTER II

Materials and methods

II.1 The computational model of hiPSC

During the thesis work the hiPSC-CM model from *Paci et al.*[19]was used It reproduces the spontaneous AP beating of atrial and ventricular-like hiPSC-CM, but for this work only the ventricular-like was considered.

A general overview is given in FigureII.1, which highlights the cell compartment, ion currents and pumps. Since the model is based on the HH formalism, the membrane potential is formulated as:

$$\begin{aligned} C\frac{dV}{dt} = &- (I_{Na} + I_{CaL} + I_f + I_{K1} + I_{Kr} + I_{Ks} + I_{to} + I_{NaCa} \\ &+ I_{NaK} + I_{pCa} + I_{bNa} + I_{bCa} + I_{NaL} - I_{stim}). \end{aligned} \tag{II.1}$$

where C is the membrane capacitance and V the membrane potential. I_{stim} is the stimulus current, which was used to replicate specific experimental drug test protocols in the original publication.

The intracellular K^+ concentration is kept constant, due to a legit approximation because the amount of K^+ transferred between intracellular and extracellular compartments is very low compared to K^+ intracellular concentration. The others ion concentrations are described as follow:

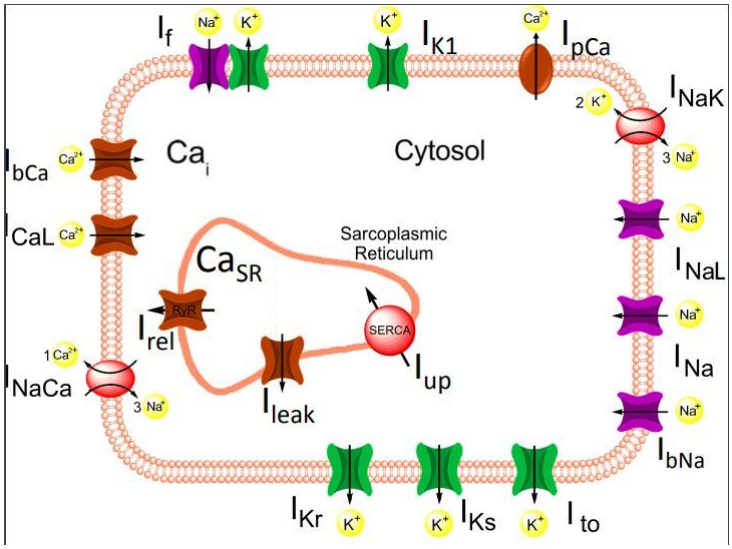

Figure II.1: : Schematic diagram of the model; image adapted from [19]

$$\frac{dNa_i}{dt} = \frac{I_{Na} + I_{bNa} + 3I_{NaK} + 3I_{NaCa}}{FV_c} \tag{II.2}$$

$$\frac{dCai_{i,total}}{dt} = I_{leak} - I_{up} + I_{rel} - \frac{I_{CaL} + I_{bCa} + I_{pCa} - 2I_{NaCa}}{FV_c} \tag{II.3}$$

$$\frac{dCa_{SR,total}}{dt} = \frac{V_c}{V_{SR}}(I_{up} - I_{rel} - I_{leak}) \tag{II.4}$$

where F represents the Faraday constant, V_c and V_{SR} are the cytosolic and sarcoplasmic volume respectively, $Ca_{i,total}$ and $Ca_{SR,total}$ are the intracellular and sarcoplasmic concentration respectively of Ca^{2+}, either free buffered.

Referring to FigureII.1, the model present:

- Ion currents: L-type Ca^{2+} current I_{CaL}, rapid delayed rectifier K^+ current I_{Kr}, slow delayed rectifier K^+ current I_{Ks}, outward transient K^+ current I_{to}, inward rectifier K^+ current I_{k1}, funny current I_f, Na^+ current I_{Na}, late Na^+ current I_{NaL}, background Ca^{2+} current I_{bCa}, background Na^+ current I_{bNa};
- Ion exchangers: Na^+/Ca^{2+} exchanger I_{NaCa};

- Pumps: Na^++/K^+ pump I_{NaK} and sarcolemmal Ca^{2+} pump I_{pCa};
- Fluxes from/to the SR: Ca^{2+} SR release I_{rel}, Serca ATP-ase pump and leakage flux I_{leak};

I_{Na}, I_{CaL}, I_f, I_{to}, I_{K1}, I_{Kr} and I_{Ks} were fitted on the experimental data from *Ma et al.*[16]. Where no experimental data were available, the ion currents were adapted referring to a previous hESC-CM model[20].

AP shapes are analytically compared using morphologic biomarkers, the AP features. In this case the following were considered:

- Cycle Length;
- Rate of spontaneous beating expressed in bpm;
- MDP: maximum diastolic potential;
- Peak: maximum voltage reached by the AP;
- APA: action potential amplitude, calculated from MDP to APA;
- V_{max}: is the maximum value of the slope during the AP upstroke;
- APD_{10}, APD_{30} and APD_{90}: action potential duration computed respectively at 10%, 30% and 90% of the repolarization;
- $Rapp_{APD}$: is a shape factor calculated as follow $\frac{APD_{30}-APD_{40}}{APD_{70}-APD_{80}}$;

In TableII.1 a AP features comparison with experimental measurement can be found.

Table II.1: Comparision between experimental and simulated ventricular AP. Experimental data are presented as: $Mean \pm SEM$

AP Features	**Unit**	**EXP**	**SIM**
Cycle Length	s	1.7 ± 0.1	1.6
Rate of spontaneous beating	bpm	35.3 ± 2.2	37.4
MDP	mV	-75.6 ± 1.2	-76.7
Peak	mV	28.3 ± 1.0	28.1
APA	mV	104 ± 1.1	104.8
$\frac{dV}{dt}max$	$\frac{V}{s}$	27.8 ± 4.8	24.4
APD_{10}	ms	74.1 ± 4.8	63.4
APD_{30}	ms	180 ± 10.7	238.9
APD_{90}	ms	414.7 ± 21.8	417.5
$Rapp_{APD}$	-	2.5 ± 0.2	3.17

II.2 Ca^{2+} dynamic and limitations of the model

The Ca^{2+} have a key role during the EC coupling, since it is needed to activate the crossbridge mechanism. As explained in Chapter 1, in order to achieve a cell contraction, a relatively huge amount of Ca^{2+} is needed in the intracellular compartment. During phase 1 of the ventricular AP, I_{CaL} activates, carrying Ca^{2+} inside the cytosol, but it is not enough to trigger the contraction. However, it is enough to activate the CICR, mechanism. The SR has Ca^{2+} sensitive receptors (ryanodine sensitive, RyR-sensitive, receptors) sensing the Ca^{2+} concentration in the cytosolwhich allow the Ca^{2+} release from the SR when they sense the intracellular Ca^{2+} increment due to I_{CaL}. This establishes a positive feedback mechanism since the more Ca^{2+} is carried inside cytosol from I_{CaL} and I_{rel}, more I_{rel} flows, causing a Ca^{2+} concentration increase, which allows the cell contraction.

The model replicates this process well but in a simplified way. Although the I_{rel} activation physiologically relies on the Ca^{2+} binding to RyR-sensitive receptors, in the model formulation, it relies directly on the I_{CaL} voltage-dependent activation variable. So I_{rel} is not directly triggered by intracellular Ca^{2+} increase. This approximation was meant to simplify the Ca^{2+} handling description, due to the lack of solid experimental data on Ca^{2+} handling in hiPSC-CM at the time the original Paci2013 model was developed. Despite it can reproduce Ca^{2+} transient, a new I_{rel} formulation is needed to obtain a more physiological behavior of the model.

II.3 Novel I_{rel} formulation

After a literature review, an accurate formulation of I_{rel} was found, from a published human atrial CM model by Koivumäki et al[21]. Based on the HH formulation, the Koivumaki model presents a novel formulation of the SR compartment and Ca^{2+} release current. The SR compartment is divded into four parts and each of them is provided with an uptake unit (I_{ip}) and a release unit (I_{rel}). This spatial discretization is meant to be a well-functioning approximation of the SR volume, since the model is integrated only along

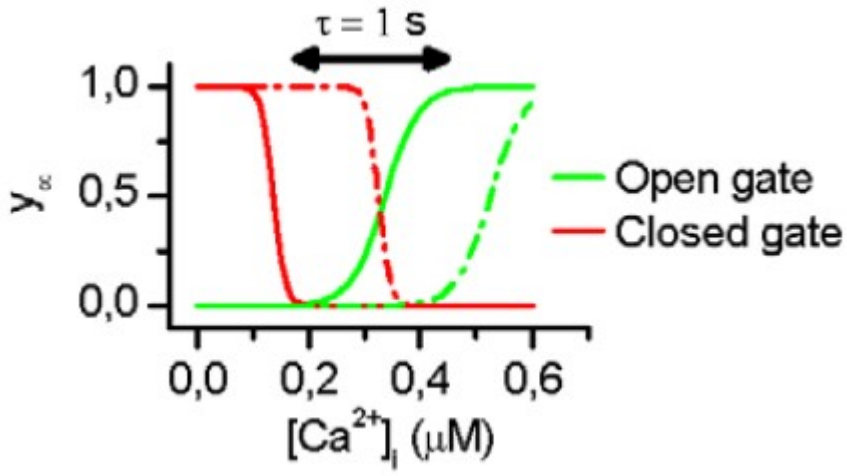

Figure II.2: role of adptation gate; figure adapted from[21]

the time dimension, allowing a realistic representation of Ca^{2+} transients. Despite this, our intention was not to replicate the whole structure of the Koivumäki model SR (since it could be not physiologically acceptable for hiPSC-CMs, due to their underdeveloped SR, different from atrial cardiomyocyte SR), but to find a suitable I_{rel} formulation which does not depend on the I_{CaL} voltage dependent activation variable. Therefore, we only used the Koivumäki I_{rel} formulation.

This novel I_{rel} formulation respect the classical HH approach and it is described by three Ca^{2+} concentration dependent gating variable: adaptation gate, open gate, closed gate. The role of the adaptation gate can be explained as follow: in FigureII.2 it is showed the probabilities of the open and closed gates dependent of I_{rel} concentration for two different state of adaptation

So, the adaptation gate can shift the point of dynamic equilibrium according to the Ca^{2+} concentration in the cytosol $[Ca^{2+}]_i$ In figure 2.3 two illustrative examples are shown: on the left column the adaptation gate is functioning, so, in presence of an reduced Ca^{2+} extrusion towards the extracellular environment, i.e. a change of the working condition, the system is able to compensate and prevent I_{rel} to shut down (this can be observed by the Ca^{2+} transient peaks, since Irel carries Ca^{2+} ions inside the intracellular

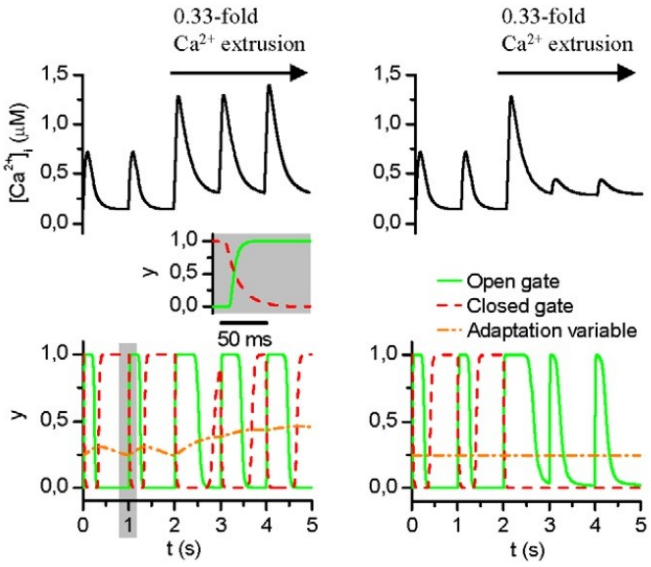

Figure II.3: : Differences betweed model with non-inhibited (left column) and inhibited (right column) adaptation gate in the Koivumäki model. The reduced Ca^{2+} extrusion (0.33-fold) was implemented by reducing by 67% I_{NaCa}, I_{pCa} and I_{up}; image adapted from [21]

compartment). On the other hand, in the right column, this compensation does not happen, because the adaptation gate is inhibited.

Compared to the Paci2013 hiPSC-CM model I_{rel} formulation, the Koivumaki one allowed us to disconnect Irel from I_{CaL}, at the price of a slightly higher computational cost, due to the introduction of two additional differentai lequations for the adaptation and the open gate (the close gate was already included in the original Paci2013 hiPSC-CM model). However, since we need to use a formulation taken from an adult CM model in a hiPSC-CM model, further steps should be followed to obtain a model properly simulating APs and Ca^{2+} transients of hiPSC-CMs. Substantial differences, such as cell volume, compartments volume, and ionic concentrations, requires a fine tuning of the mathematical I_{rel} formulation parameters.

Furthermore, the availability of experimental data of Ca^{2+} transient give the opportunity to fit I_{rel} parameters in a more accurate form. This procedure can be achieved in different ways, such as a manual parameter tuning, but we chose to use an automatic procedure based on an optimization framework,

that will be discussed in the next section of this chapter.

II.4 Experimental data of Ca^{2+} transients

The Ca^{2+} experimental data used to tune the I_{rel} parameters were obtained by measures on actual hiPSC-CMs, performed at BioMediTech (www.biomeditech.fi), a joint institute of Biomedical Sciences and Engineering of the Tampere University of Technology and the University of Tampere (Finland). Such data consist in a set of Ca^{2+} transient features concerning magnitude and duration values. Measurements were made with calcium imaging. This kind of measurement is widely used to show the Ca^{2+} status of a cell through some Ca^{2+} sensitive fluorescent dyes. Those molecules are able to change their fluorescence properties after binding selectively to Ca^{2+} ions. The variation of this fluorescent signal, acquired with a CCD camera, can describe the amount of Ca^{2+} inside a cell. In particular, to quantify the Ca^{2+}, is necessary to perform a system calibration since the Ca^{2+} transient amplitude is relative to the basal fluorescence of the dyes, i.e. the fluorescence observed when no Ca^{2+} transient occurs.

Therefore, it is not possible knowing the absolute value of features concerning magnitude (e.g. amplitude of the transient expressed as mM), unless performing the calibration of the dye. Unfortunately, such calibration is usually not done by the biologists who recorded Ca^{2+} data. For this reason, only time-domain features are considered, as listed below:

- **Time to peak**: time needed to reach maximum Ca^{2+} concentration value;
- **Maximum rise slope:** maximum value of the slope reached by the Ca^{2+} transient;
- **Rise time 10% to 90%:** time that occurs to rise from the 10% to the 90% of transient amplitude;
- **Rise slope 10% to 90%:** average slope from 10% to the 90% of transient amplitude;

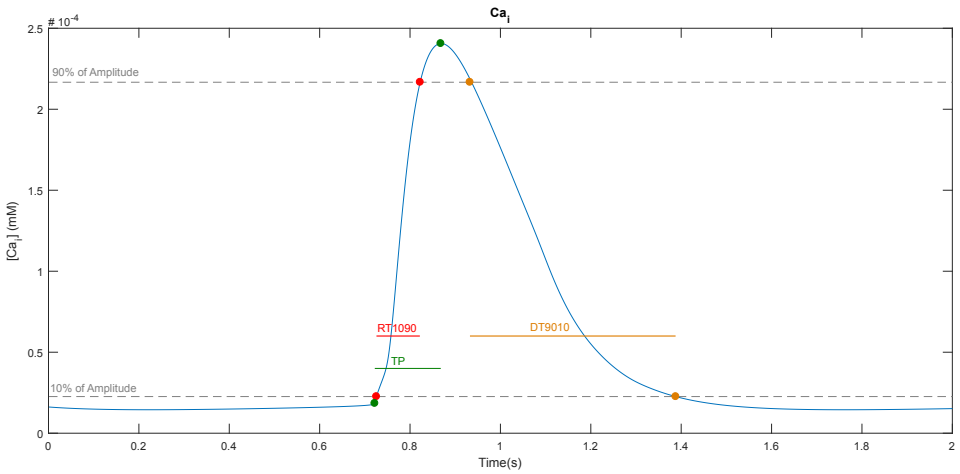

Figure II.4: Time domain biomarker of a Ca^{2+} transient. The Maximum Rise Slope is maximum value of the slope between the two green dots. Rise time from 10 to 90% and Decay slope from 90 to 10% are calculated as an average of the slope between the red and yellow dots respectively.

- **Decay time 90% to10%:** time that occurs to decay from the 90% to the 10% of transient amplitude;
- **Decay slope 90% to 10%:** average slope from 90% to the 10% of transient amplitude;
- **Event frequency:** transient frequency;

In FigureII.4 is illustrated how are the biomarkers calculated from a single Ca^{2+} transient.

II.5 Cell Classification

The in vitro measurements were performed on a 13 hiPSC-CM cells, several times for each cell (from 2 to 5 times) and are presented as $Mean \pm SD$. Since no information about the cell phenotype (e.g. atrial-like or ventricular-like) was given and the model we replace I_{rel} is the ventricular-like version of the Paci2013 hiPSC-CM model, a classification of experimental data is needed.

Due to the lack of any prior information about the cell phenotypes, the most suitable choice is an unsupervised classifier.

K-means algorithm is used in order to perform a clusterization into two class, atrial and ventricular-like. Three Ca^{2+} transient features are used as discriminating factors for the algorithm: Decay slope 90% to 10%, Decay tau, Event frequency. The reason behind this choice can be explained considering some differences between atrial and ventricular spontaneous activities. In [22][16] it is shown that atrial-like cells have a more rapid spontaneous beating activity, resulting in a higher basal beating frequency. Ca^{2+} transient follow this faster spontaneous activity, so a discrimination based on beating frequency and decay slope results to be the most accurate one. In addition to the Decay slope 90% to 10% and Event frequency, described in the previous section, for clustering we used also the Decay tau feature, i.e. the time constant of the exponential curve used to fit the Ca^{2+} transient decay.

II.6 The Optimization framework

The optimization procedure consists in using a framework able to tune automatically the model parameters. The main idea come from a previous published work [23] used for the same purpose but for a different cell model. Shortly, the framework calculates a cost function and tries to minimize it, giving as result an optimal parameter set. The framework is implemented in Matlab and it is based on the fminsearch function, a powerful tool for function optimization.

As shown in FigureII.5, the workflow of the algorithm consists in an iterative process that starts from an initial parameter set. The choice of the target parameters is crucial for the following reasons. A too large set of parameters is difficult or impossible to optimize, so it is important to choose the most relevant parameters. Moreover, since experiment-based parameter tuning was already done for several ions current formulations during the Paci2013 hiPSC-CM model development[19], only parameters of the few currents for which experimental data were not available at the time of the development of the Paci2013 model should be chosen, in addition to the I_{rel} formulation

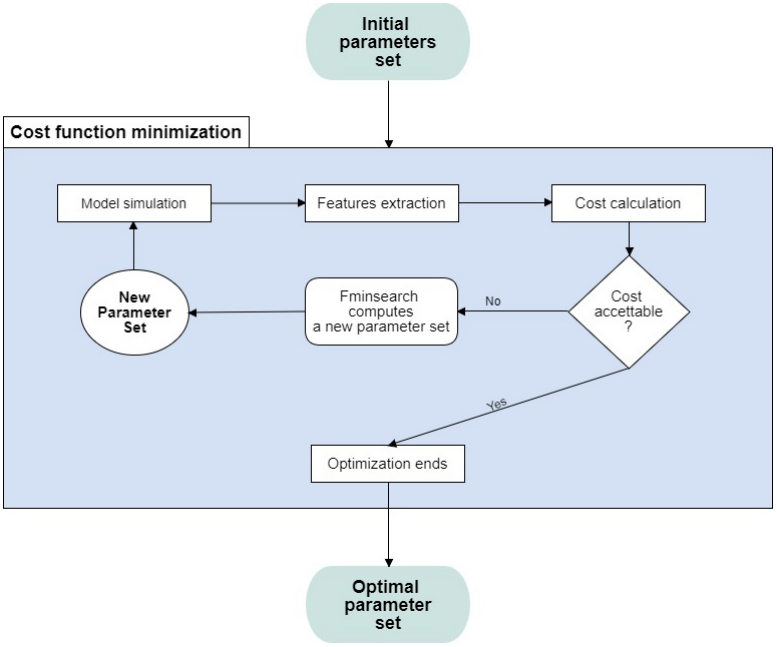

Figure II.5: 5 Working principle of the optimization framework.

ones.

After these considerations, 11 parameters were chosen as the most appropriate ones, as listed below:

- $\mathbf{V_{max.up}}$**:** maximum conductance of the SERCA pump, also called I_{up};
- $\mathbf{K_{up}}$**:** parameter that regulate the equilibrium of the SERCA pump;
- $\mathbf{K_{NaCa}}$**:** maximum conductance of I_{NaCa};
- $\mathbf{alpha_{NaCa}}$: parameter that regulates the equilibrium of I_{NaCa};
- $\mathbf{P_{Nak}}$ maximum conductance of I_{NaKl};
- $\mathbf{V_{leak}}$: maximum conductance of I_{leak};
- $\mathbf{G_{irel}}$ maximum conductance of I_{rel};
- **RyRa1** parameter of the steady-state variable in the I_{rel} formulation;
- **RyRa2** parameter of the steady-state variable in the I_{rel} formulation;

- **RyRahalf** half-activation concentration of the I_{rel} adaptation gate;
- **RyRohalf** half-activation concentration of the I_{rel} open gate;
- **RyRchalf** half-activation concentration of the I_{rel} closed gate;

The next step that the framework requires is to define a cost function. This function is based on this formula:

$$C = \sum_i \frac{\Delta_i}{\sigma_{i;exp}} * w_i \tag{II.5}$$

Where C is the cost, $\sigma_{i;exp}$ is the SD of the i^{th} experimental feature, w_i is the weight assigned to the i^{th} feature and Δ_i is the difference between the experimental and simulated ith feature. Δ_i can assume:

- 0, if the simulated feature is within the experimental range $Mean \pm SD$;
- $|Feat_{sim} - \sigma_{i;exp}|$,where $Feat_{sim}$ is the value of the feature simulated., if $Feat_{sim}$ is outside the experimental range $Mean \pm SD$;

This function will give an output cost proportional to how much the simulated data are close to the experimental ones. So the overall cost is given by the sum of each single feature contribution properly weighted. This contribution will increase in a linear way if the feature is outside the experimental $Mean \pm SD$, otherwise the cost is null. The set of target features used for the optimization process consists in two parts:

- the AP features from[16], which were used to tune the original version of the Paci2013 hiPSC-CM model. This feature set is necessary to keep the in silico AP shape consistent with the experimental hiPSC-CM APs.
- the Ca2+ features computed on the in vitro Ca2+ transients, explained in section 2.4.

Furthermore, in order to calculate these features from simulated traces of APs and Ca^{2+} transients a novel features extraction function was created

ad hoc and it is formed by two parts. The first part is able to extract a time window relative to the last 5 APs from the whole model simulationc, since the features must be extracted when the system reaches the steady state. On the other hand, the second part calculate the features for each of these 5 APs (and also 5 Ca^{2+} transients, since for each AP correspond a Ca^{2+} transient) and average them.

II.7 Model Validation through currents blocker simulations

During the experimental recording accomplished by Ma et al on hiPSC-CM, current blockers measurements were done. Those measurements consist in using drugs that are able to selectively block an ion channel, thus resulting in an AP shape variation. Depending on which current blocker is used, the AP shape changes in different ways, since each ion activates in different AP phases, as shown in Chapter 1. Since the goal of this thesis is to develop a model which accurately reproduces the electrophysiological behaviour of hiPSC-CM, simulations of the effects of current blockers provide a useful form of validation on the model.

The simulated current blockers presented here are tetrodotoxin (TTX), nifedipine (Nifed) and E4031 that are selective current blocker for INa, ICaL and IKr respectively. To simulate these blockers, the maximum conductance of the target current is reduced according to the dose-response curves, which are the experimental quantification of the blocking effect on the current targeted by the blocker. We simulated the same experimental protocol used in Ma et al: pacing rate fixed at 1 Hz, depolarizing pulses of 5 ms with an amplitude of 550 pA for Nifed and E4031 and 750 pA for TTX.

CHAPTER III

Results

All the results obtained during this thesis work will be illustrated in this chapter. The experimental data gathering and classification will be shown. Then the optimization framework results will be presented as well as the electrophysiological behaviour of the model with the new I_{rel} formulation implemented and tuned.

III.1 Experimental Calcium data classification

The experimental measurements were performed on a set of hiPSC-CM wild type using calcium imaging technique. The Ca^{2+}+ traces were acquired with a variable frame rate from 9 Hz to 26 Hz and then analysed with *ClampFit* software. Since no information about the cell culture lineage is available, it is not possible to discriminate them into atrial or ventricular-like. Therefore we used an unsupervised classification tool in order to attempt to discriminate between atrial and ventricular-like phenotypes and to have a better and accurate set of experimental measurement for the next steps of this thesis. The data come from a set of 13 cells which the features are extracted from. The measurements are performed N times on each cell and then the results are presented as$Mean \pm SD$. In Table 3.1 it is reported an example data

Table III.1: Example of experimental data sheet. The features are: TP=time to peak ; $\frac{dCa_i}{dt}max$=maximum rise slope ; RT1090= rise time from 10 to 90% ; RS1090= rise slope from 10 to 90%; DT1090= decay time from 90 to 10%; DS9010= decay slope from 90 to 10% ; FREQ= event frequency. N is the number of single cell measurement repetition

Feature	**Unit**	**Mean**	**SD**	**N**
TP	ms	274.286	56.25	14
$\frac{dCa_i}{dt}max$	$\frac{Mol}{s}$	2.22	0.51	14
RT1090	ms	165.49	30.48	13
RS1090	$\frac{Mol}{s}$	0.93	0.62	13
DT9010	ms	238.542	31.75	14
DS9010	$\frac{Mol}{s}$	-0.673	0.235	14
Frequency	Hz	1.406	0.180	13

sheet of a single cell.

After the experimental data collection, a Matlab script was set up to perform the classification with the *K-Means* function. The algorithm needs the target features to classify our set of cells and, as we described in the previous chapter we used the *Decay slope 90% to 10%*, *Decay tau* and *Event frequency*, since time-domain features represent, in our situation, the best discriminating factors. Furthermore *K-means* requires the features to be normalized first and, after this operation, we started the classification procedure. This procedure is mandatory since our variables have incomparable units (e.g *Decay tau* in ms and *Event frequency* in Hz) and they need a standardization to be equally classified. The results of the algorithm are reported below (FigureIII.1,FigureIII.2). For a clear and understandable presentation of the results, is was chosen to show only two features for each figure, although the features-space is 3 dimensional (*Decay slope 90% to 10%, Decay tau, Event frequency*).

K-means divided the 13 cells into two classes that we associated with the phenotypes ventricular-like (9 cells) and atrial-like (4 cells). After classification, we can represent them with their original measurement units (Fig-

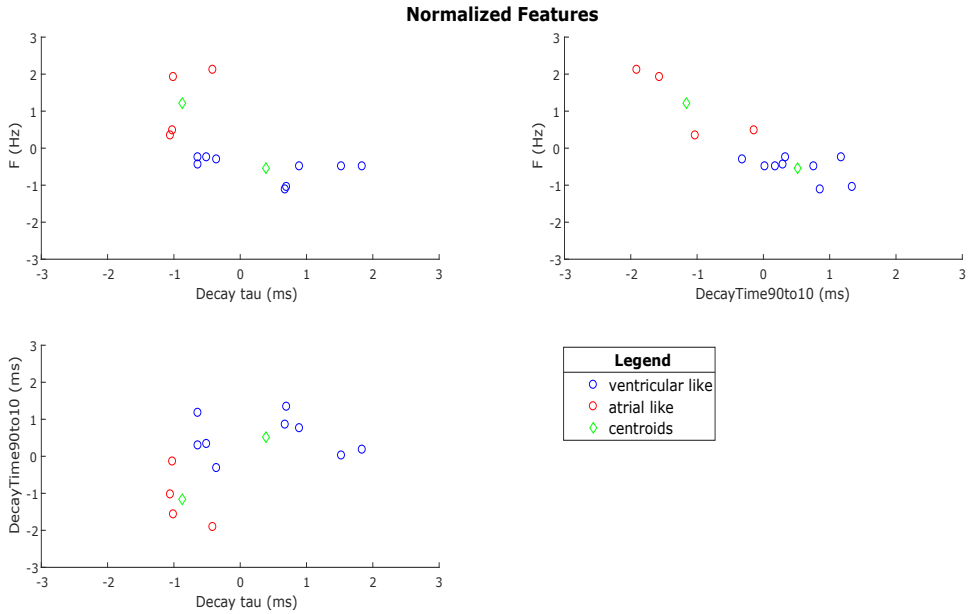

Figure III.1: Distribution of normalized features into the two-dimensional features space. In green are also reported the centroids of the clusters

ureIII.2).

Looking at the figures with original values, the cells classified as atrial-like present generally a higher beating frequencies, faster decay constants as well as shorter Decay Time. On the contrary, the cells classified as ventricular-like have slower beahviour: lower beating frequencies, slower decay constants and longer Decay time. This results are coherent with the experimental findings([16][22]) and considering that no a priori information was given to classify the data set so we can hypothesize this result as reliable.

After classification, mean and standard deviation were extracted from the 9 ventricular-like cells to use them in the optimization framework. Results are presented in TableIII.2.

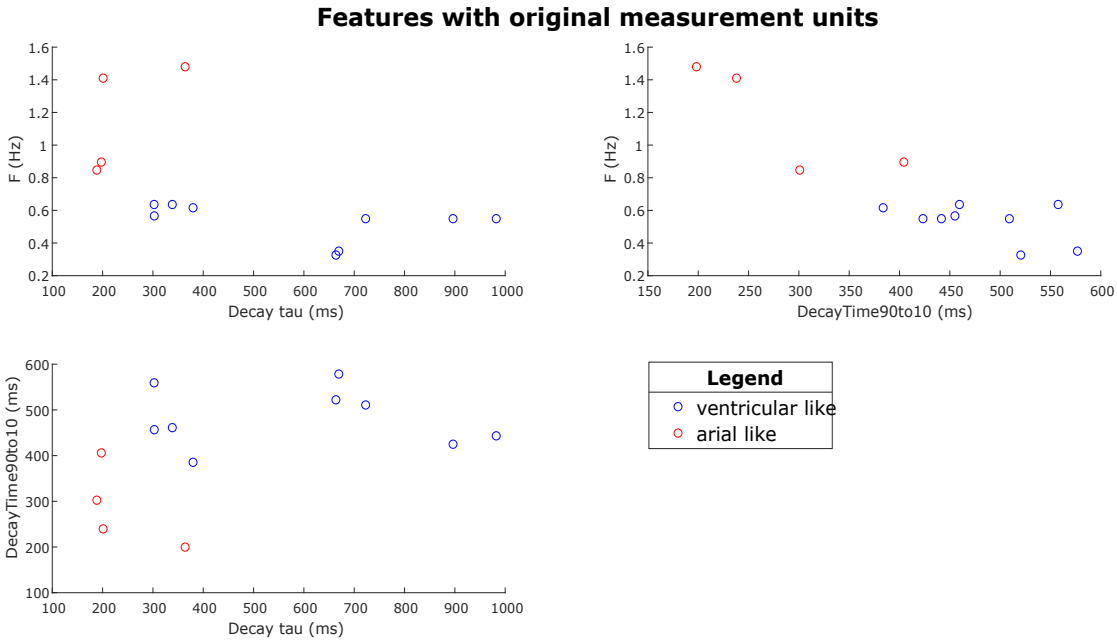

Figure III.2: Distribution of normalized features into the two-dimensional features space.

Table III.2: : Mean and SD of the biomarkers recorded on the 9 cells classified as ventricular-like.

Feature	**Unit**	**Mean**	**SD**
TP	ms	399	105.4339
$\frac{dCa_i}{dt}max$	$\frac{Mol}{s}$	3.5583	1.6786
RT1090	ms	28	55.83
RS1090	$\frac{Mol}{s}$	1.1221	1.2413
DT9010	ms	481	64.0934
DS9010	$\frac{Mol}{s}$	-0.8119	0.5706
Frequency	Hz	0.5277	0.1151

Table III.3: Initial parameter set used in the optimization framework.

Parameter name	Value
$V_{max,up}$	0.56064
K_{up}	0.00025
K_{NaCa}	5978
$alpha_{NaCa}$	2.8571
P_{NaK}	2.2958
V_{leak}	0.00044
G_{rel}	64
RyRa1	0.505
RyRa2	0.427
RyRahalf	0.29
RyRohalf	0.22
RyRchalf	0.02

III.2 Optimization framework results

At this point, the result from the experimental data classification can be used in the optimization framework cost function to compare also the Ca^{2+} features simulated by the model.

As explained in the previous chapter, the cost function uses both AP and Ca^{2+} features to compute a cost. In addition to the Ca2+ features, we used the same experimental AP features used to develop the hiPSC-CM Paci 2013 model from *Ma et al*[16].

Referring to FigureII.5 in the previous chapter, the framework needs an initial parameter set to start the optimization procedure. Since the aim is not to change drastically the model behaviour, but only to tune formulation limited set of parameters, it was chosen to start the optimization procedure with the same parameters of the Paci2013 model. On the other hand, concerning the new Irel formulation parameters, it was used the same parameters set of the original published paper III.3.

The overall cost is calculated as the sum of all the single feature cost. This value is proportional to how much the features is outside the experimental range $Mean \pm SD$. Despite the Ca^{2+} features were already cal-

culated as Ca^{2+}, AP features from *Ma et al.*[16] are presented as $Mean \pm SEM$(Standard error of the Mean). Since it was chosen to use the SD for the cost function the SEM needs to be converted. The formula below expresses the relationship between SEM and SD:

$$SD = \frac{SEM}{\sqrt{N}}$$

Where N is the number of the observations(34).

Furthermore, each single feature contribution to the overall cost is weighted by a scalar factor that allow to control and decide which features is worth to be more considered or not. In TableIII.4 a summary of the features used in the first step of the optimization procedure is reported: the initial value of the cost function is 9.78.

Table III.4: Summary of the biomarker used to initialize the cost function.

Feature	**Unit**	**Mean**	**SD**	**Weight**
APA	mV	104	6.2225	1
MDP	mV	-75.6	6,7882	2
$Cyclelength$	ms	1700	565.6854	2
$\frac{dV}{dt}max$	$\frac{V}{s}$	27.8	27.1529	1
APD_{10}	ms	74.1	27.1529	1
APD_{30}	ms	180	60.5283	1
APD_{10}	ms	414.7	123.319	1
$RAPP_{apd}$	-	2.5	1.1313	1
TP	ms	399	105.4339	0.2
$\frac{dCa_i}{dt}max$	$\frac{Mol}{s}$	3.5583	1.6786	0.2
$RT1090$	ms	28	55.83	0.2
$RS1090$	$\frac{Mol}{s}$	1.1221	1.2413	0.2
$DT9010$	ms	481	64.0934	0.2
$DS9010$	$\frac{Mol}{s}$	-0.8119	0.5706	0.2
$Frequency$	Hz	0.5277	0.1151	0.2

Table III.5: : Optimized parameter set. It is also shown the starting parameter set and the percent variation.

Parameter name	**Optimized**	**Original**	**Variation**
$V_{max,up}$	0.5785	0.56064	+3%
K_{up}	0.00027	0.00025	+7%
K_{NaCa}	4868	5978	−22%
$alpha_{NaCa}$	2.8095	2.8571	−1%
P_{NaK}	2.4819	2.2958	+7%
V_{leak}	0.0004661	0.00044	+5%
G_{rel}	64.805	64	+2%
RyRa1	0.4809	0.505	−2%
RyRa2	0.4541	0.427	+6%
RyRahalf	0.3001	0.29	+4%
RyRohalf	0.2154	0.22	−2%
RyRchalf	0.0204	0.02	+2%

Finally, the optimization was started. Due to the high computational cost, the optimization procedure last for several hours and, at the end, reached a result with a cost of 0.9. The optimal parameter set found by the framework is reported in TableIII.5.

The previous table allows to see the changes between the initial and the optimized parameter set. The variation goes from a 22% of the starting value in case of K_{NaCa} to the 1% of $alpha_{NaCa}$. In the next section it will be shown how the optimized parameter set affect the model electrophysiological behaviour.

III.3 New hiPSC-CM ventricular-like model

Finally, we can present the hiPSC-CM ventricular like model with the optimized parameter set.

The simulated AP traces and the major ionic currents are shown in FigureIII.3 during spontaneous electrical activity. The figures are obtained after 800 seconds of simulation to let the model reach the steady state. Further-

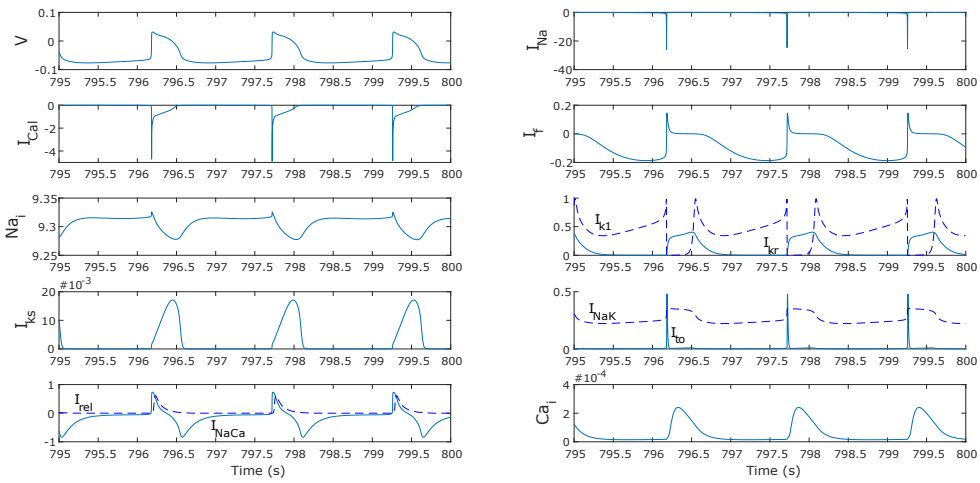

Figure III.3: : spontaneous Ap, ionic currents and ionic concentrations at model steady state. The measurement units are expressed in: Volts for the AP; Ampere/Farad for the ionic currents; millimolar for the ionic concentrations.

more, in Tab 3.6 there is the comparison between the simulated biomarkers and the experimental biomarkers computed by Ma et al. for the APs and at Biomeditech for the Ca^{2+} transients.

The table shows that the model is able to well reproduce the experimental biomarkers. All the AP features, except the APD_{30}, are within the range Mean±SD. Moreover, the Ca^{2+} features $\frac{dCa_i}{dt}$max, RS1090, DS9010 are within the experimental intervals as well. Referring to TableII.1, is also useful to make a comparison between the new and the original model: the APD_{30} is not reproduced by both, but now, with the optimized parameters, the new hiPSC-CM model can successfully reproduce the APD_{10} and $RAPP_{APD}$.

In order to have a better overview about the new changes introduced in the Paci2013 model, a comparison between the AP and intracellular Ca^{2+} traces produced by the old and new version of the model are presented below. In fig FigureIII.4 it can be observed that the new model AP trace has a slightly higher maximum peak voltage (+11%) but the same maximum diastolic potential . On the other hand, Ca^{2+} transient in fig 3.7 shows that

Table III.6: Comparison between experimental biomarkers and those simulated by the hiPSC-CM ventricular-like model with the optimized parameter set values.Data are presented as Mean± SD

Feature	**Unit**	**EXP**	**SIM**
APA	mV	104±6.2225	107.9639
MDP	mV	-75.6±6,7882	-76.6234
$Cyclelength$	ms	1700±565.6854	1539
$\frac{dV}{dt}max$	$\frac{V}{s}$	27.8±27.1529	24.7196
APD_{10}	ms	74.1±27.1529	77.6250
APD_{30}	ms	180±60.5283	250.125
APD_{10}	ms	414.7±123.319	400.25
$RAPP_{apd}$	-	2.5±1.1313	2.6583
TP	ms	399±105.4339	149
$\frac{dCa_i}{dt}max$	$\frac{Mol}{s}$	3.5583±1.6786	3.1790
$RT1090$	ms	28±55.83	78
$RS1090$	$\frac{Mol}{s}$	1.1221±1.2413	2.3027
$DT9010$	ms	481±64.0934	335.25
$DS9010$	$\frac{Mol}{s}$	-0.8119±0.5706	-0.5392
$Frequency$	Hz	0.5277±0.1151	0.6497

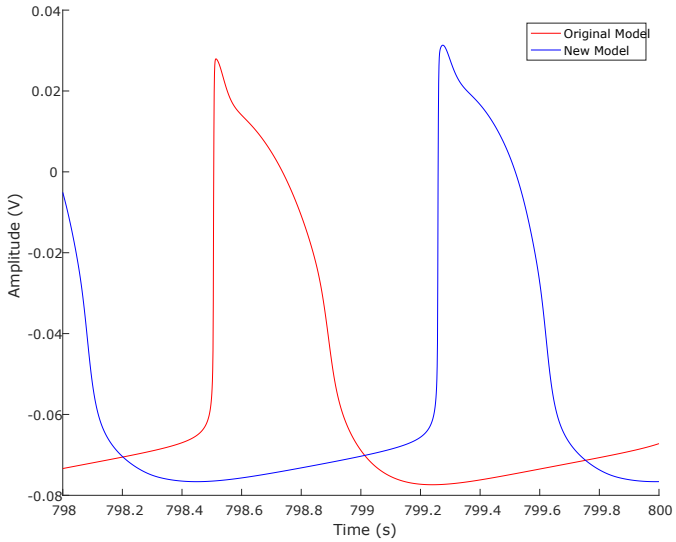

Figure III.4: Spontaneous AP comparison after 800 s simulation.

the systolic Ca^{2+} is lower in the new model (-13%) while the diastolic Ca^{2+} is not significantly affected by the changes in the model.

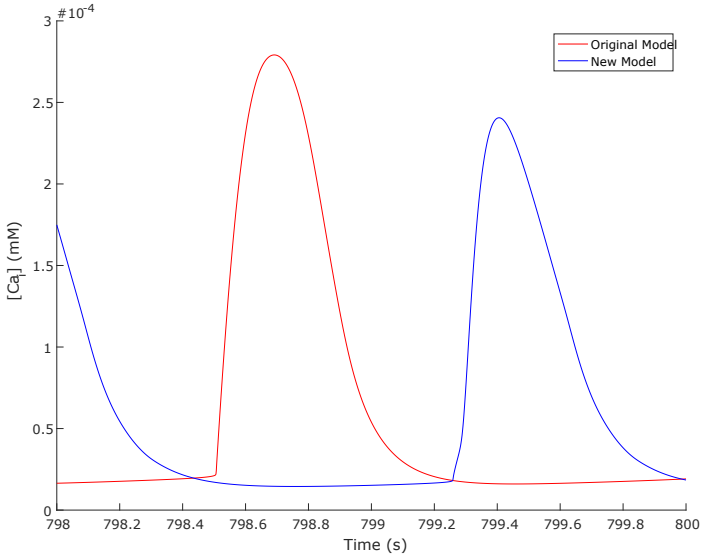

Figure III.5: Spontaneous Ca^{2+} transient comparison after 800 s simulation.

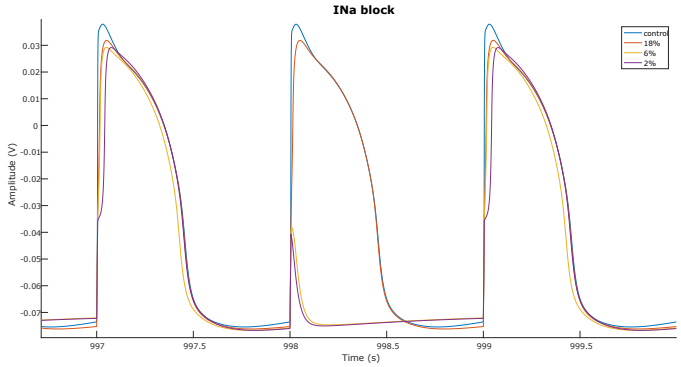

Figure III.6: I_{Na} blocker simulation

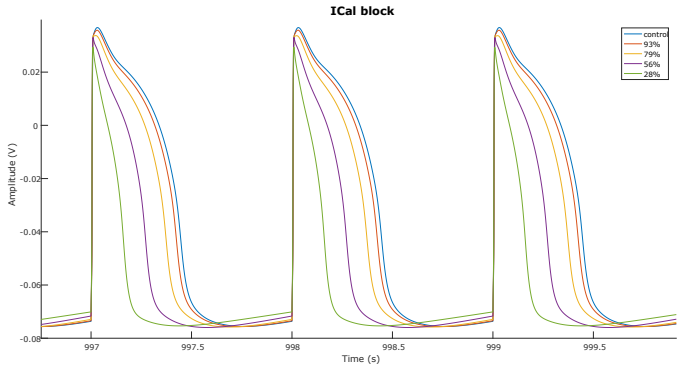

Figure III.7: I_{CaL} blocker simulation

III.4 Selective current blockers simulation

The TTX simulation consist in reproducing the effect of 3 ,10 ,30 μM of TTX, that reduces the maximum conductance of I_{Na} (G_{Na}) by 18%, 6%, 2% respectively (FigureIII.6) The effect on are evaluated with a simulation of 3,10,30,100 nM of Nifed that reduces the I_{CaL} maximum conductance (G_{CaL}) by 93%,79%,56%,28% respectively (FigureIII.7). Finally, a simulation of 30 and 100 nM of E4031 is performed by reducing the maximum I_{Kr} conductance by 77% and 50% respectively ((FigureIII.8)). All these reduction percentages were estimated from the dose-response curves reported in[19].

In TableIII.7 the quantitative effects of current blocker on APD90 and dV/dt max are reported. In FigureIII.6 it can be observed the effect of I_{Na}

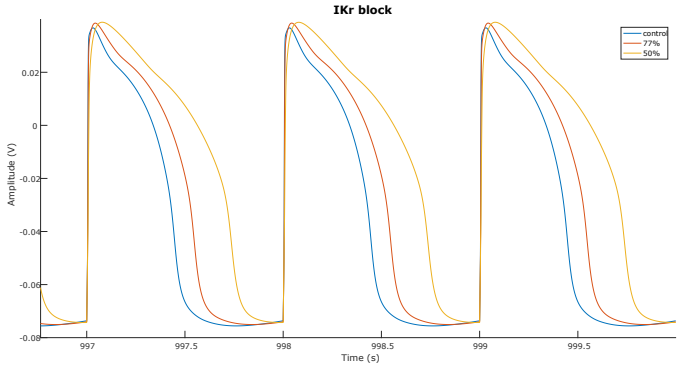

Figure III.8: I_{Kr} blocker simulation

block. I_{Na} is the main responsible current for the AP upstroke so its inhibition shifts in time the AP peak. Also, in case of 6% and 2% of G_{Na} reduction, I_{Na} is not enough to trigger the AP for all the external stimulation pulses.

In FigureIII.7, the effect of I_{CaL} reduction can be observed in a AP shortening as I_{CaL} has the role of sustaining the AP plateau.

In FigureIII.8 I_{Kr} block produces an AP lengthening since I_{Kr} is the responsible of the membrane repolarization. Qualitatively the simulated APs are consistent with the experimental findings in [16]. With the introduction of the new I_{rel} formulation, the model is still able to well reproduce the current blocker experiments.

Table III.7: Quantification of current blocker effects on $\frac{dV}{dt}$max and APD_{90}

AP Features	**Experiments**		**Simulations**	
$\frac{dV}{dt}$ max	TTX $3\mu M$	41.2±11%	18%G_{Na}	23%
	TTX $10\mu M$	16.7±1.8%	6%G_{Na}	/
	TTX $30\mu M$	61.8±2%	2%G_{Na}	/
APD_{90}	Nifed 3nM	89.4±1%	93%G_{CaL}	96.53%
	Nifed 10nM	78.4±4.4%	79%G_{CaL}	85.9%
	Nifed 30nM	74±2.3%	56%G_{CaL}	65.7%
	Nifed 100nM	58.2±5.4%	28%G_{CaL}	43.8%
APD_{90}	E4031 30nM	140.3±7.6%	77%G_{Kr}	120%
	E4031 100nM	170.4±13.6%	50%G_{Kr}	157.9%

CHAPTER IV

Conclusions

The aim of this thesis was to improve the Ca^{2+} handling mechanisms, in particular the Ca^{2+} release from the SR, in the already published Paci model of the AP of hiPSC-CMs[19]. Such model is the first hiPSC-CM model available in literature and it has been used for many applications, such as the comparison of the effects of drugs on hiPSC-CMs and adult cardiomyocytes[24] or the evaluation of the electrophysiological variability on the long QT 3 mutation and drug effects in hiPSC-CMs[25]. However, the Paci model suffered from a very simplified description of the Ca^{2+} handling, which was inherited from the TenTusscher 2004 model of adult ventricular cardiomyocyte [17].

Specifically, the accompishments achieved during this thesis work consist in:

- the adaptation of the optimization framework, published in [23], to the hiPSC-CM modelling problem, which can be used also for further improvements of the hiPSC-CM model;
- an improved and more realistic I_{rel} formulation, which accurately reproduces the biological mechanism of I_{rel} activation;
- a new model parameter set chosen by the optimization framework by means of AP literature data and Ca^{2+} transient traces experimentally

recorded at BioMediTech;

- an unsupervised classifier to process the experimental Ca^{2+} transient data, in particular to infer their ventricular or atrial-like origin.

- a new version of the Paci hiPSC-CM model which exploits the new I_{rel} formulation, but still is able to reproduce all the experimental data it was able to reproduce in its original formulation.

The introduction of the new Irel formulation, that has a cytosolic Ca^{2+} concentration-dependant activation gate, allows the Paci2013 to overcome the limit imposed by the old I_{rel} formulation, which was dependent on the I_{CaL} voltage-dependent activation gate.

The optimization procedure lead to another achievement: the model is now able to reproduce two more AP features: APD_{10} and $RAPP_{APD}$. Considering the relevance of $RAPP_{APD}$ in *Ma et al.*[16], the result can be considered a valuable achievement, since this feature is used to discriminate between atrial-like and ventricular-like.

Moreover, this thesis work has provided, with the optimization framework, a powerful and suitable tool to be used in model parameter tuning.

One of the major limitation encountered during this thesis work is represented by the high variability of hiPSC-CM. This can be attributed to several reasons that can space from experimental environment differences in the hiPSC-CM culturing phase to substantial differences among patients from which hiPSC-CM are produced. Our optimization process is based on dataset that came from two different culturing cells lines; we used the dataset from *Ma et al*[16] to compute the cost for AP features and the dataset from Biomeditech to compute the cost for the Ca^{2+} features. Since no information about the Ca^{2+} traces was given in dataset from *Ma et al* and, conversely, no information was given about the AP traces in the dataset from Biomeditech, we are not able to detect and quantify if there are some substantial differences between the two datasets. Despite this, it can be observed (TableIII.4) that the AP Interval and the Ca^{2+} Event Frequency, after the conversion in Hz from bpm, present similar values of 0.5882 and 0.5277 respectively, but still

there are no other evidences about the two-dataset similarity. We took into account this uncertainty on experimental data by choosing different weights in the cost function. Basically, we decided to assign a higher weight to AP feature compared to Ca^{2+} features.

The high variability in hiPSC-CM put some limits in cardiac modelling because it became difficult to reproduce with a single model formulation, datasets that come from different cell lines. Since the Paci2013 was developed according to a single data source (i.e. the dataset from *Ma et al*[16]) and, in literature, Ca^{2+} dynamic in hiPSC-CM are still under study and is still not well-known, we decided to assign higher value to AP features to prevent the optimization framework from finding an inconsistent parameter set.

Another limitation could be represented by the lack of information about phenotype of the cell used for Ca^{2+} transient measurement. In *Ma et al*[16] the discriminating criterion used to classify cells between atrial-like and ventricular-like was the $RAPP_{APD}$: cells with this ratio > 1.5 were classified as ventricular-like. In our case, data provided by Biomeditech concerns only Ca^{2+} features so we were not able to use the same criterion. Unfortunately, the new hiPSC-CM model is not able to reproduce all the Ca^{2+} features. In particular, differences between the experimental and simulated values of TP, RT1090 and DT9010 suggest that the high variability of hiPSC-CM should be taken into account. Such variability could make very difficult conjugating in the same in silico model in vitro data from two different sources (*Ma et al*[16] and BioMediTech).

In the end, using an automatic procedure to tune the model parameter brings clear advantages as well as some limitations. Compared to a manual parameter tuning, the optimization framework offers the possibility to test a wider range of parameter sets in a relatively short time, but there is the possibility to find a not fully physiologically consistent parameter set at the end of the optimization process. The procedure is based on a function minimization through *fmisearch* tool, so there is the risk to encounter a local cost function minimum instead of a global minimumor if the minimization problem itself could not be solved in an analytic way. There should be always a well-ponderate preliminary setting to allow the procedure giving a consistent

result. This setting includes: the right choice of initial parameter set, the optimum trade-off of the target parameters and the proper weight choice.

In conclusion, in this work we showed that a carefully used optimization framework allowed to exploit new Ca^{2+} experimental data to improve the Paci hiPSC-CM model. This opens also prospective for future works, i.e. to further improve this new formulation of the Paci model by means of other mechanisms, such as the inositol 1,4,5-trisphosphate-dependent Ca^{2+} release. However, the reliability of cardiac modelling is strictly related to the availability of experimental data: therefore, another expectation is that in future more in vitro studies will be conducted to allow a continuous improvement of in silico hiPSC-CM models.

Acknowledgements

All this thesis work was done at the Tampere University of Technology (TUT) and at the BioMediTech Institute located in Tampere, Finland. The research period lasted six months and gave me the opportunity to be part of a team in a very stimulating enviroment.
I thank Prof. Jari Hyttinen, head of the Computational Biophysics and Imaging Group at TUT and BioMediTech, for having provided all the infrastructures and materials used for this thesis.
Special thanks to Dr. Michelangelo Paci, postdoctoral researcher at TUT and BioMediTech, for being primarly a friend and the co-supervisor of the thesis and for having supported and introducted me to the electrifying world of cardiac modelling.
Finally, I would like to thank Prof. Stefano Severi for his support and for the overall supervision of this thesis.

Bibliography

[1] Smith A.; *A glossary for stem-cell biology.* Nature. 2006;

[2] Scholer RH.,*The Potential of Stem Cells: An Inventory.* In Knoepffler N, Schipanski D, Sorgner SL (eds.), Humanbiotechnology as Social Challenge; Ashgate Publishing. 2007;

[3] Thomson JA. *Embryonic Stem Cell Lines Derived from Human Blastocysts.* Science. 1998;

[4] Takahashi K, Tanabe K, Ohnuki M, Narita M, Ichisaka T, Tomoda K, Yamanaka S. *Induction of pluripotent stem cells from adult human fibroblasts by defined factors.* Cell. November 2007;

[5] Yu J, Vodyanik MA, Smuga-Otto K, Antosiewicz-Bourget J, Frane JL, Tian S, Nie J, Jonsdottir GA, Ruotti V, Stewart R, Slukvin II, Thomson JA.*Induced Pluripotent Stem Cell Lines Derived from Human Somatic Cells.*.Science. 2007;

[6] Meregalli M, Farini A. *Stem Cell Therapy for Neuromuscular Diseases*

[7] **Site** https://emedtravel.wordpress.com/2013/01/08/revolutionary-human-stem-cell-trial;

[8] Pekkanen-Mattila M. *Cardiomyocyte Differentiation from Human Pluripotent Stem Cells.* Tampere University Press, 2010;

[9] Pekkanen-Mattila M, et al.*Substantial variation in the cardiac differentiation of human embryonic stem cell lines derived and propagated under the same conditions–a comparison of multiple cell lines*;

[10] Takahashi T, Lord B, Schulze PC, Fryer RM, Sarang SS, Gullans SR, Lee RT. *Ascorbic acid enhances differentiation of embryonic stem cells into cardiac myocytes.* Circulation, April 2003;

[11] Morita H, Wu J, Zipes DP. *The qt syndromes: long and short.*. The Lancet. 2008;

[12] D. A. Tehran. *Physiology: an integrated approach.* in http://www.tesionline.it/v2/appunto-sub.jsp?p=73&id=250;

[13] Passini E. Population of model: the imporatnce of of biological variability an how to include it in cardiac computational modeling. Alma mater studiorum University of Bologna. Seminar. 2014;

[14] Walker CA, Spinale F. *The structure and function of the cardiac myocyte: a review of fundamental concepts.* The Journal of Thoracic and Cardiovascular Surgery. 1990;

[15] Bettiol E, Sartiani L, Chicha L, Krause KH, Cerbai E, Jaconi ME.*Fetal bovine serum enables cardiac differentiation of human embryonic stem cells.* Differentiation research in biological diversity. October 2007;

[16] Ma J, Guo L, Fiene S, Anson B, Thomson J, Kamp T, Kolaja K, Swanson B, January C. *High purity human-induced pluripotent stem cell-derived cardiomyocytes: electrophysiological properties of action potentials and ionic currents.* Am J Physiol Heart Circ Physiol. 2011;

[17] ten Tusscher KHWJ, Noble D, Noble PJ, Panlov AV. *A model for human ventricular tissue.* Am J Physiol Heart Circ Physiol. 2004;

[18] Hodgkin A, Huxley A. *A quantitative description of membrane current and its application to conduction and excitation in nerve.* J Physiol Lond. 1952;

[19] Paci M, Hyttinen J, Aalto-Setaa.*Computational Models of Ventricular and Atrial-Like Human Induced Pluripotent Stem Cell Derived Cardiomyocytes.* Annals of Biomedical Engineering. 2013;

[20] Paci M, *Computational modelling of human stem cell-derived cardiomyocytes.* Alma Mater Studiorum University of Bologna. Doctoral thesis. 2013;

[21] Koivumali J, Korhonen T, Tavi P.*Impact of Sarcoplasmic Reticulum Calcium Release on Calcium Dynamics and Action Potential Morphology in Human Atrial Myocytes: A Computational Study.* Computational Biology. 2011;

[22] Josowitz R,Lu J,Falce C, D'Souce SL, et al. *Identification and Purification of Human Induced Pluripotent Stem Cell-Derived Atrial-Like Cardiomyocytes Based on Sarcolipin Expression.* PLOS Journal. 2014;

[23] Fabbri L. *Estrazione automatica di parametri fisiologici da registrazioni di potenziali d'azione cardiaci.* Alma Mater Studiorum University of Bologna. 2013;

[24] Paci M,Hyttinen J,Rodriguez B, Severi S. *Human induced pluripotent stem cell-derived versus adult cardiomyocytes: an in silico electrophysiological study on effects of ionic current block.* British Journal of Pharmacology. 2015;

[25] Paci M, Passini E, Rodriguez B, Severi S, Hyttinen J. *Phenotypic variability in LQT3 human induced pluripotent stem cell-derived cardiomyocytes and their response to anti-arrhythmic pharmacological therapy: an in silico approach.* Heart Rhythm. 2017;

[26] Gunaseeli L, Doss Mx,Antzelevitch C. *Induced pluripotent stem cells as a model for accellerated patients and disease specific drugs discovery*;

[27] Sollano J, et al. *The Economics of Drug Discovery and the Ultimate Valuation of Pharmacotherapies in the Marketplace.*

;